AFRL-RV-PS-
TP-2021-0098

AFRL-RV-PS-
TP-2021-0098

DPRK NUCLEAR EXPLOSION YIELDS FROM TELESEISMIC MODELING

Thorne Lay

University of California Santa Cruz
Department of Earth and Planetary Sciences
1156 High Street
Santa Cruz, California 95064

21 November 2021

Final Report

APPROVED FOR PUBLIC RELEASE; DISTRIBUTION IS UNLIMITED.

AIR FORCE RESEARCH LABORATORY
Space Vehicles Directorate
3550 Aberdeen Ave SE
AIR FORCE MATERIEL COMMAND
KIRTLAND AIR FORCE BASE, NM 87117-5776

DTIC COPY

NOTICE AND SIGNATURE PAGE

Using Government drawings, specifications, or other data included in this document for any purpose other than Government procurement does not in any way obligate the U.S. Government. The fact that the Government formulated or supplied the drawings, specifications, or other data does not license the holder or any other person or corporation; or convey any rights or permission to manufacture, use, or sell any patented invention that may relate to them.

This report was cleared for public release by AFMC/PA and is available to the general public, including foreign nationals. Copies may be obtained from the Defense Technical Information Center (DTIC) (http://www.dtic.mil).

AFRL-RV-PS-TR-2021-0098 HAS BEEN REVIEWED AND IS APPROVED FOR PUBLICATION IN ACCORDANCE WITH ASSIGNED DISTRIBUTION STATEMENT.

//SIGNED//	//SIGNED//
_____	_____
Dr. Raymond J. Willemann	For: Erin N. Pettyjohn, Chief
Program Manager/AFRL/RVB	AFRL Geospace Technologies Division

This report is published in the interest of scientific and technical information exchange, and its publication does not constitute the Government's approval or disapproval of its ideas or findings.

REPORT DOCUMENTATION PAGE

Form Approved
OMB No. 0704-0188

Public reporting burden for this collection of information is estimated to average 1 hour per response, including the time for reviewing instructions, searching existing data sources, gathering and maintaining the data needed, and completing and reviewing this collection of information. Send comments regarding this burden estimate or any other aspect of this collection of information, including suggestions for reducing this burden to Department of Defense, Washington Headquarters Services, Directorate for Information Operations and Reports (0704-0188), 1215 Jefferson Davis Highway, Suite 1204, Arlington, VA 22202-4302. Respondents should be aware that notwithstanding any other provision of law, no person shall be subject to any penalty for failing to comply with a collection of information if it does not display a currently valid OMB control number. **PLEASE DO NOT RETURN YOUR FORM TO THE ABOVE ADDRESS.**

1. REPORT DATE *(DD-MM-YYYY)*	**2. REPORT TYPE**	**3. DATES COVERED** *(From - To)*
21-11-2021	Final Report	27 Sep 2018 – 23 Sep 2021

4. TITLE AND SUBTITLE
DPRK Nuclear Explosion Yields from Teleseismic Modeling

5a. CONTRACT NUMBER
FA9453-18-C-0065

5b. GRANT NUMBER

5c. PROGRAM ELEMENT NUMBER
62601F

6. AUTHOR(S)
Thorne Lay

5d. PROJECT NUMBER
1010

5e. TASK NUMBER
EF133214

5f. WORK UNIT NUMBER
V1H9

7. PERFORMING ORGANIZATION NAME(S) AND ADDRESS(ES)
University of California Santa Cruz
Department of Earth and Planetary Sciences
1156 High Street
Santa Cruz, CA 95064

8. PERFORMING ORGANIZATION REPORT NUMBER

9. SPONSORING / MONITORING AGENCY NAME(S) AND ADDRESS(ES)
Air Force Research Laboratory
Space Vehicles Directorate
3550 Aberdeen Avenue SE
Kirtland AFB, NM 87117-5776

10. SPONSOR/MONITOR'S ACRONYM(S)
AFRL/RVBN

11. SPONSOR/MONITOR'S REPORT NUMBER(S)
AFRL-RV-PS-TR-2021-0098

12. DISTRIBUTION / AVAILABILITY STATEMENT
Approved for public release; distribution is unlimited. (AFRL-2022-0039 dtd 05 Jan 2022)

13. SUPPLEMENTARY NOTES

14. ABSTRACT
Seismic yields for the six declared underground nuclear tests at the North Korean test site are estimated. Absolute calibration is obtained by modeling broadband P wave ground displacements observed at teleseismic distances for the 2017 event for a granite source medium using the Mueller-Murphy explosion model, adjusting the site attenuation parameter and the pP lag time and relative amplitude in order to match the waveshapes and average amplitude. Relative to the resulting yield estimate for the 2017 event of 230 ± 50 kt for a frequency independent average $t^* = 0.78 \pm 0.03$, 4-Hz amplitude signals from the other five events are modeled using the same explosion model and attenuation operator, giving estimates in the range of 2.6 to 18.8 kt for the events from 2006 to 2016. This gives absolute-amplitude based yield estimates for all six events. The modeling uses a simple half-space or a plane-layered medium, frequency-independent attenuation, and the apparently significant effects of non-elastic behavior of the pP phase (delayed in time relative to elastic predictions) for the 2017 event are modeled in a simplified fashion. Broader band seismic wave estimates of the yields are obtained using short-period waveform equalization by the process of intercorrelation, involving cross-convolution with the Green's functions for two events, tied in absolute amplitude to the direct modeling results. Generally consistent relative yield estimates for the six events are obtained for a procedure that uses simple half-space media for the Green's functions and allows for non-elastic delay times of pP. Estimates of yields are in the range 1.4 to 250 kt for preferred values with burial depths constrained by event location in the mountain. Direct estimates of the Green's functions are obtained by deconvolving the source time functions from the foregoing analysis from regional broadband recordings, and layered 1D velocity structures are developed to match the deconvolved traces. Azimuthal variations in the deconvolved Green's functions and the 1D models indicate differences at northerly azimuths versus southerly azimuths, consistent with geological variations above the sources. The inferred 1D structures (both uniform and azimuthally varying) are then used in intercorrelations, producing yield estimates that prove to be very similar to those obtained for simple half-space models.

15. SUBJECT TERMS
explosion modeling, North Korean nuclear tests, intercorrelation, yield estimation, site attenuation correction

16. SECURITY CLASSIFICATION OF:			**17. LIMITATION OF ABSTRACT**	**18. NUMBER OF PAGES**	**19a. NAME OF RESPONSIBLE PERSON**
a. REPORT	**b. ABSTRACT**	**c. THIS PAGE**			Dr. Raymond J. Willemann
Unclassified	Unclassified	Unclassified	Unlimited	24	**19b. TELEPHONE NUMBER** *(include area code)*

This page is intentionally left blank.

Approved for public release; distribution is unlimited.

TABLE OF CONTENTS

Section **Page**

Approved for public release; distribution is unlimited.

LIST OF FIGURES

Figure **Page**

LIST OF TABLES

Table **Page**

1. SUMMARY

Seismic yields and explosion source time functions for the six declared underground nuclear tests at the North Korean test site are estimated. Absolute calibration is obtained by modeling numerous broadband P wave ground displacements and 4-Hz initial P wave amplitudes observed at teleseismic distances for the 2017 event using a Mueller-Murphy granite source medium explosion model, adjusting the site attenuation parameter and the pP lag times in order to match the waveshapes and average amplitudes. The modeling uses a simple half-space or a plane-layered medium, frequency-independent attenuation, and parameterizes the apparently significant effects of non-elastic behavior of the pP phase (delayed in time relative to elastic predictions). The broadband waveforms and event-averaged 4-Hz amplitudes for the 2017 event are well modeled, giving a yield estimate for the 2017 event of 230 ± 50 kt for a frequency independent average $t^* = 0.78 \pm 0.03$ s. This result is sensitive to an inferred large deviation of the pP lag time from an elastic value, attributed to the extensive damage zone expected for this very large shallow explosion. The average 4-Hz amplitude signals from the other five events are modeled using the same explosion model and attenuation operator, giving estimates in the range of 2.6 to 18.8 kt for the events from 2006 to 2016. This procedure obtains absolute-amplitude based yield estimates and source time functions for all six events. Broader band seismic wave estimates of the yields are next obtained using short-period waveform equalization by the process of intercorrelation, involving cross-convolution with the Green's functions for two events, tied in absolute amplitude to the direct modeling results. Generally consistent relative yield estimates for the six events are obtained for intercorrelations that use simple half-space media for the Green's functions and allow for non-elastic delay times of pP. Estimates of yields are in the range 1.4 to 250 kt for preferred values that have burial depths constrained by event location in the mountain. The source time functions estimated by this procedure are then deconvolved from regional Pn observations to extract direct estimates of the Pn Green's functions. Very consistent signals are found for station MDJ (to the north) for all but the 2006 event, and a 1D layered elastic model is determined that matches the pPn above-source structural interactions for the larger events. This model produces similar apparent delayed pPn arrivals to the parametric non-elastic half-space models used in the initial analysis. The Pn Green's functions are much simpler at INCN (to the south) and are well modeled by an elastic half-space, as is the signal at MDJ for the 2006 event. The 1D structures are then used in intercorrelations for all teleseismic observations. Very similar results are found using the layered MDJ model for all azimuths, or when azimuthally varying the source velocity model to have a 1D structure for stations to the south, and/or using a 1D structure for the 2006 event at all azimuths. The relative yield estimates appear to be quite stable with respect to specific 1D source structure, but the full effects of 3D elastic and non-elastic structure are yet to be considered.

Approved for public release; distribution is unlimited.

2. INTRODUCTION

Reliable estimation of nuclear explosion yields for new test sites for which we do not have data from a direct calibration experiment presents the difficult problem of calibration of seismological properties of the crust and upper mantle around the site. Prior to the Joint Verification Experiment, Soviet test sites were calibrated by detailed waveform analysis of teleseismic recordings of underground tests, resulting in m_b-Yield relationships that were subsequently validated by the JVE direct calibration. A similar challenge now exists for empirical calibration of the nuclear explosions conducted by the Democratic People's Republic of Korea (North Korea). Current methods for yield estimation for this test site largely rely on transporting m_b-Yield relationships from calibrated test sites to this uncalibrated site. This is very uncertain given the lack of seismicity in North Korea from which seismological properties such as the mantle t* bias can be directly determined. In order to calibrate the seismic recordings of the North Korean tests, we use waveform and signal amplitude modeling approaches that draw upon explosion and attenuation model parameterizations that are well established from prior experience in seismic analysis of signals for other test sites.

3. TECHNICAL APPROACH

Regional and teleseismic P wave recordings for the six underground DPRK nuclear tests have been modeled to obtain estimates of the absolute and relative yields of the six explosive devices using seismic waveform modeling methods. Modeling of broadband P wave ground motions for the 3 September 2017 nuclear test has been performed, initially for plane-layered Green's functions, along with parametrically allowing for non-elastic pP delays times and amplitudes. The trade-offs between explosion yield, burial depth and pP behavior, and site attenuation factor (t*) have been explored and partially resolved by optimizing the simultaneous fit to far-field broadband P wave amplitudes and waveforms. The effects of pP interference and burial depth are suppressed by also modeling the absolute amplitude of 4-Hz, high-pass filtered P wave seismograms for the first 0.25 s of ground motion, as this interval precedes the expected arrival of pP. This combined forward modeling analysis provides an absolute yield estimate for the 2017 event, allowing estimates of yields from 4-Hz amplitude measures for the preceding 5 events to be placed on a self-consistent absolute yield basis. This work is discussed in detail in Chaves et al. (2018).

Relative waveform equalization by a procedure called intercorrelation (e.g., Lay et al., 1984; Lay, 1985) has also been applied to large global data sets of short-period P wave recordings to determine the relative burial depths and yields of the six DPRK tests, tied to the absolute yield modeling for the 2017 event. We use explosion source functions parameterized by the Mueller-Murphy source model for a granite source medium, which are fully specified by the yield and burial depth. Analysis utilizing elastic half space Green's functions has been completed and published during this contract. Effects of non-elastic behavior in the source region are evaluated

by allowing for non-elastic pP delay times and amplitudes in the intercorrelations. The procedure thus provides robust estimates of relative source strength with explicit correction for yield scaling and burial depth variations. The absolute yield estimates are dependent on connection to the yield estimates for a given test site t* value noted above. Spectral ratios of regional Pn recordings are compared to predictions for the absolute source models (source functions prescribed by yields and burial depths), to validate the differential yield estimates. This work is discussed in detail in Voytan et al. (2019).

The overall analysis in these two publications provides estimates of the yields and t* bias for the North Korean test site, enabling calibration of the DPRK m_b-Yield relationship (for any self-consistent set of measured m_b values) for the test site directly, rather than relying on highly problematic transport of m_b-Yield relationships from other test sites. There are two large uncertainties associated with the waveform modeling. These are (1) the topography at the source region is expected to cause enhancement and azimuthal variations in free surface pP reflections for elastic structures (e.g., Avants, 2005; Stevens et al., 2018), and (2) the shallow depth of the large 2017 event resulted in extensive damage around the source and nonlinear interaction with the free surface, which affects the pP amplitudes and timing. While the modeling and intercorrelation procedures parameterize for first-order effects of pP behavior, it is not clear how much bias may exist in the results.

4. RESULTS AND DISCUSSION

Initially we had planned to implement an existing 3D spectral element code to allow rigorous inclusion of surface topography into the intercorrelation procedure for this contract, but this plan was disrupted by the pandemic impacts on hiring a suitable postdoc (visa issues in particular), and limited access to the computational assets at LLNL where the code was to be installed. Because intercorrelation equalizes signals from two events at a given station, for which any shared azimuthal pattern in the Green's functions is common to both signals, it is likely that an extensive computation of Green's functions for all possible source locations in the 3D structure to a large number of teleseismic and regional stations for frequencies from 0.5 to 5.0 Hz will actually not change the results very much. Simple tests of imposed azimuthally varying pP time and amplitude for parameterized half-space Green's functions prove very stable as long as the sources share the same azimuthal patterns, but clearly it is desirable to extend the intercorrelation to 3D Green's functions in the future. Doing so usefully will require information on the subsurface structure, rather than simply assuming topography on a half space. Accounting for non-elastic effects is even more challenging, as this is very yield dependent and detailed material properties around the sources are required (and not available).

In completing this contract, an intermediate approach was adopted, seeking to directly estimate the body wave Green's functions for the six explosions at regional distance stations that have sufficient bandwidth to provide stable estimates. The key observations are vertical component Pn

arrivals for stations MDJ (azimuth, ϕ ~ 7°, distance, D ~ 366 km), INCN (ϕ ~ 206°, D ~ 477 km), and BJT (ϕ ~ 266°, distance ~ 1097 km). An important issue is the stability of the signals over the large range of yields, given the likely variation in near source damage effects. This was appraised by deconvolving the available signals for all events from the signal for the much larger 2017 event, essentially treating the smaller events as empirical Green's functions due to their shorter duration source time functions and very similar paths to the station. The results for MDJ are shown in Figure 1, for signals band-pass filtered between 0.2 and 4 Hz.

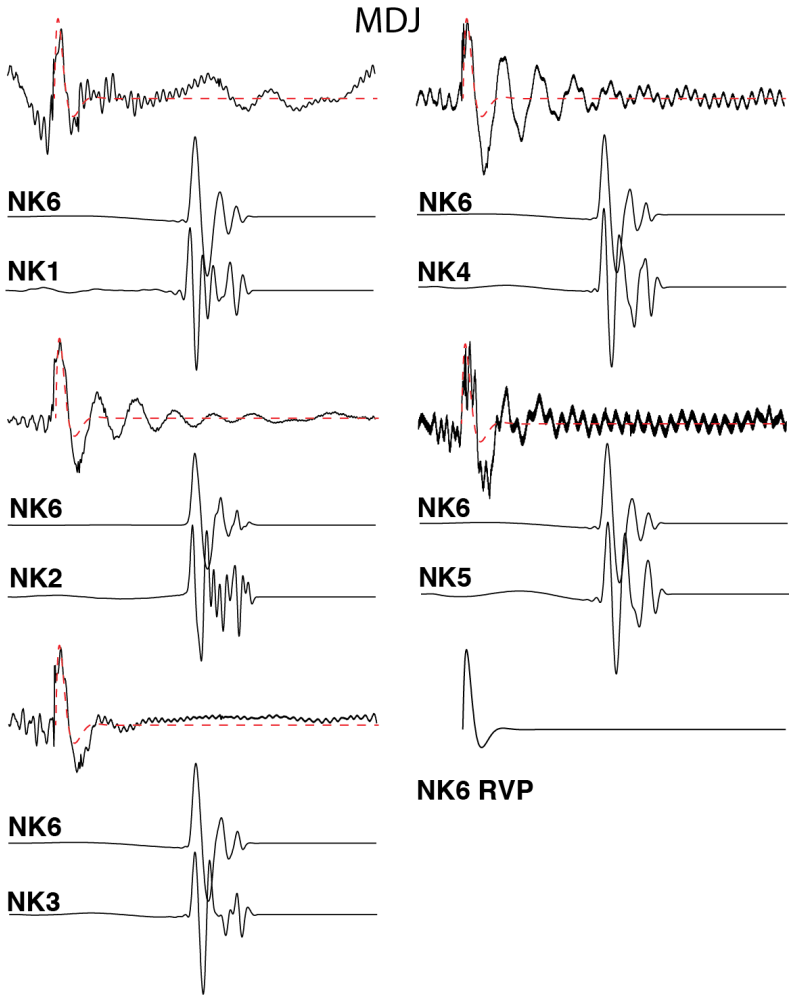

Figure 1. Deconvolution of Pn signals at station MDJ for the 2017 (NK6) event by the signals for events in 2006 (NK1), 2009 (NK2), 2013 (NK3), 2016a (NK4) and 2016b (NK5). *The estimated reduced velocity potential (RVP) for the final model for NK6 in Voytan et al. (2019) is shown at the lower right and superimposed on the 5 deconvolved traces (red dashed traces).*

If the events had identical depths and propagation effects, the deconvolutions should isolate the source function (RVP) for the 2017 (NK6) event. The comparisons with the estimated RVP for NK6 suggest that the first pulse shape and width is actually well recovered, but the first

downswing is consistently larger than expected, indicating some anomalous behavior for the 2017 event. Corresponding deconvolutions for INCN are shown in Figure 2. These show very good agreement with the predicted RVP for NK6, without strong downswings as seen at MDJ.

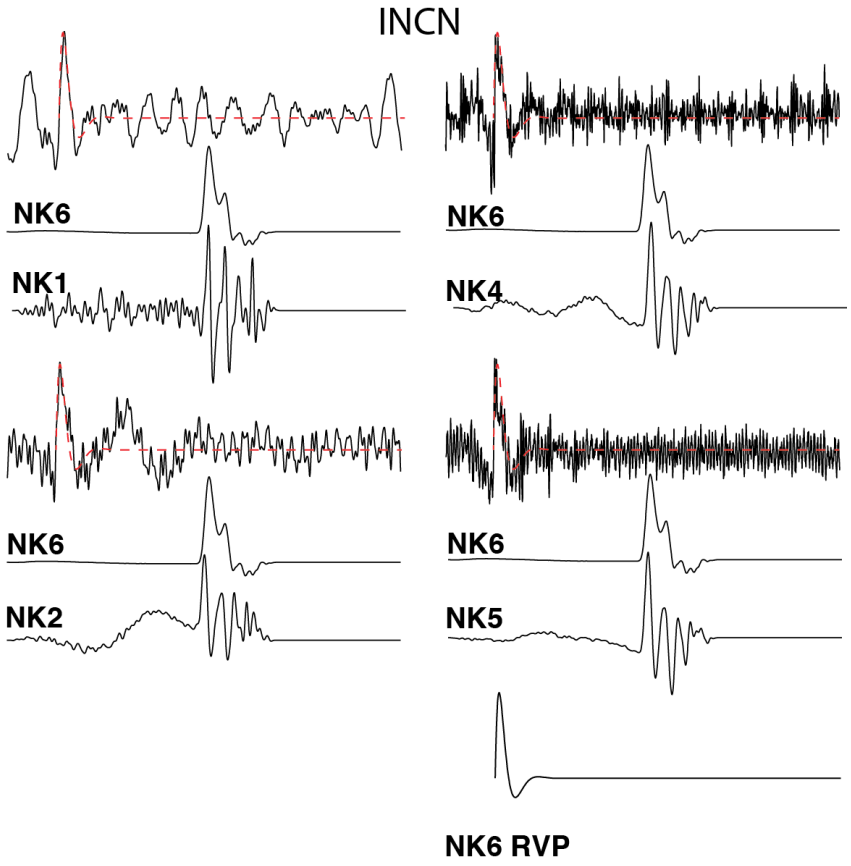

Figure 2. Deconvolution of Pn signals at station INCN for the 2017 (NK6) event by the signals for events in 2006 (NK1), 2009 (NK2), 2016a (NK4) and 2016b (NK5). *The estimate reduced velocity potential (RVP) for the final model for NK6 in (Voytan et al. 2019) is shown at the lower right and superimposed on the deconvolved traces (red dashed traces).*

The general consistency of the predicted RVP for NK6 with the first pulse of the deconvolutions at the regional stations, motivated an effort to extract the actual Green's function for each signal (rather than canceling it out as in the deconvolutions in Figures 1 and 2). We use the preferred estimates of the yields and burial depths for the six events from Voytan et al. (2018) to compute RVP signals and deconvolve them from the Pn signals for each available recording at MDJ, INCN, and BJT. The RVP signals are convolved with a constant Q t* operator of 0.05 s to suppress high frequency noise. The procedure is illustrated in Figure 3 for station MDJ.

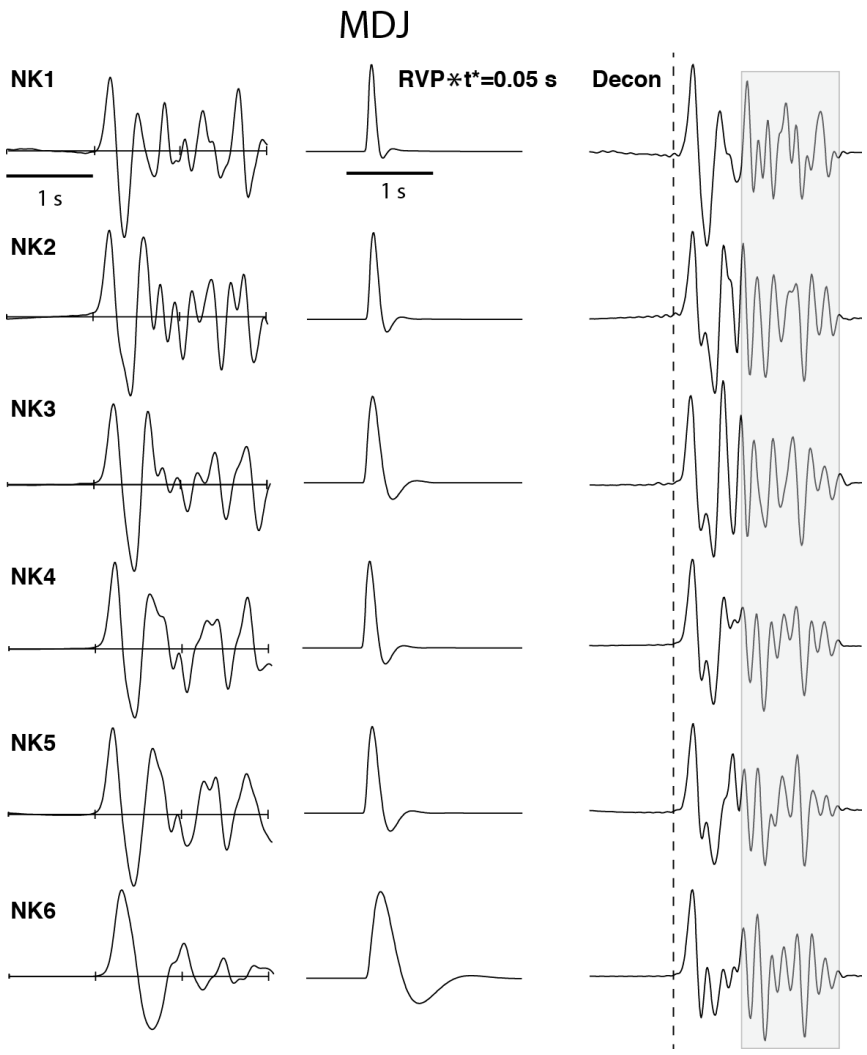

Figure 3. Deconvolution of the Pn recordings for all six events at MDJ by the RVP estimated for each source for the preferred models in Voytan et al. (2019). *Slight filtering with a t*=0.05 s operator is applied to the RVPs. The first second of the deconvolved traces show the Pn+pPn interval, with similar dovetailed waveforms in the first second of the Green's functions of the five larger events. Fairly stable path complexities in the later coda are also seen (shaded interval).*

It is encouraging that the simple signals are found in the first second of the deconvolutions, with a dovetail feature in the downswings of the five larger events suggesting similar pPn depth-phase complexity, while NK1 has a simple downswing. Coherent features in the deconvolutions are seen after 1 s, and these likely are stable crustal reverberations on the paths to MDJ.

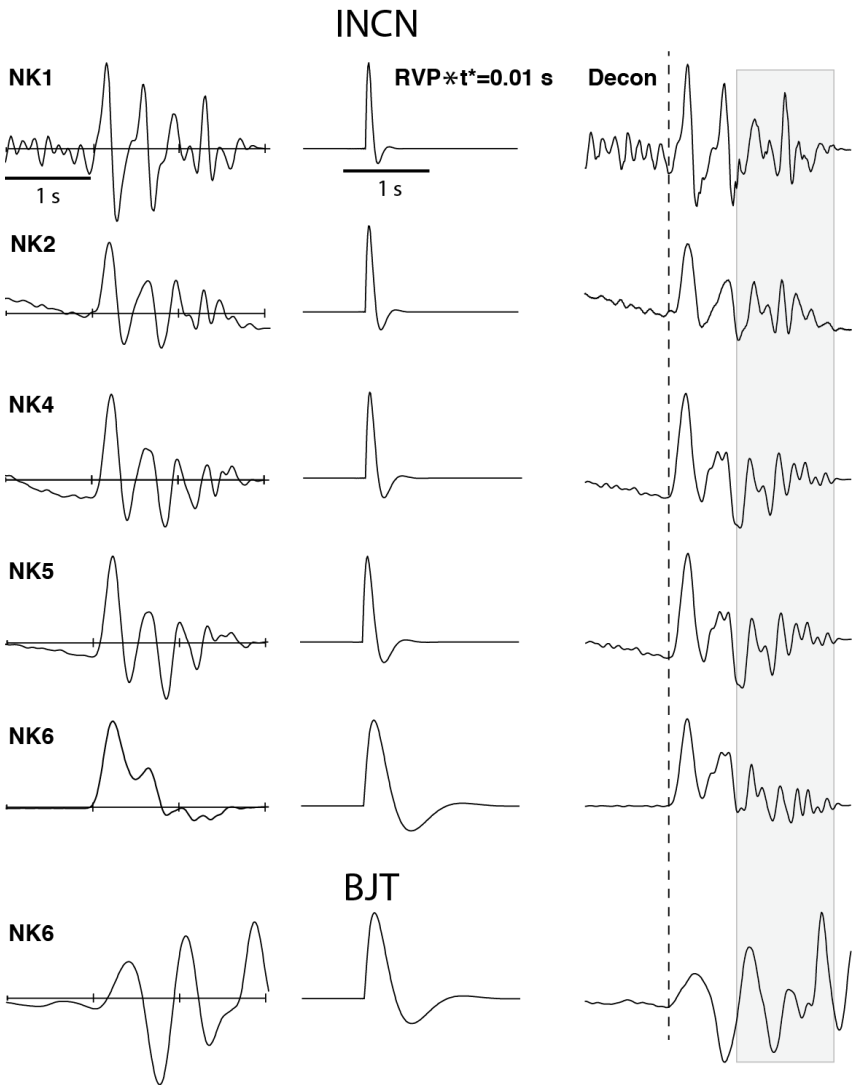

Figure 4. Deconvolution of the Pn recordings for all six events at INCN and BJT by the RVP estimated for each source for the preferred models in Voytan et al. (2019). *The first second of the deconvolved traces show the Pn+pPn interval, with similar waveforms with no overshoot in the first second of the Green's functions of the INCN recordings. NK1 is again distinctive in appearance. BJT, a large-distance Pn signal, has a very different Green's function reflecting the long propagation. Fairly stable path complexities in the later coda are also seen (shaded interval).*

Corresponding deconvolutions for INCN and BJT (only the record from NK6 has sufficient signal-to-noise ratio for this large distance Pn signal) are shown in Figure 4. The INCN Green's functions are stable and quite similar (NK1 has a stronger second upswing), with no indication of the dovetail feature apparent at MDJ, while the deconvolution for BJT has distinct appearance intermediate to that for MDJ and INCN, with smoothed signal reflecting the large distance of this Pn observation.

The deconvolutions in Figures 3 and 4 indicate a large degree of stability of the Green's functions at a given station for the five larger events, with strong azimuthal variation. The empirically-derived Pn Green's functions can be compared with those for the previous intercorrelation analysis, as shown in Figure 5 for MDJ and Figure 6 for INCN and BJT. The simple half-space Green's functions do not account for the dovetail seen at MDJ, and underestimate the downswing amplitude.

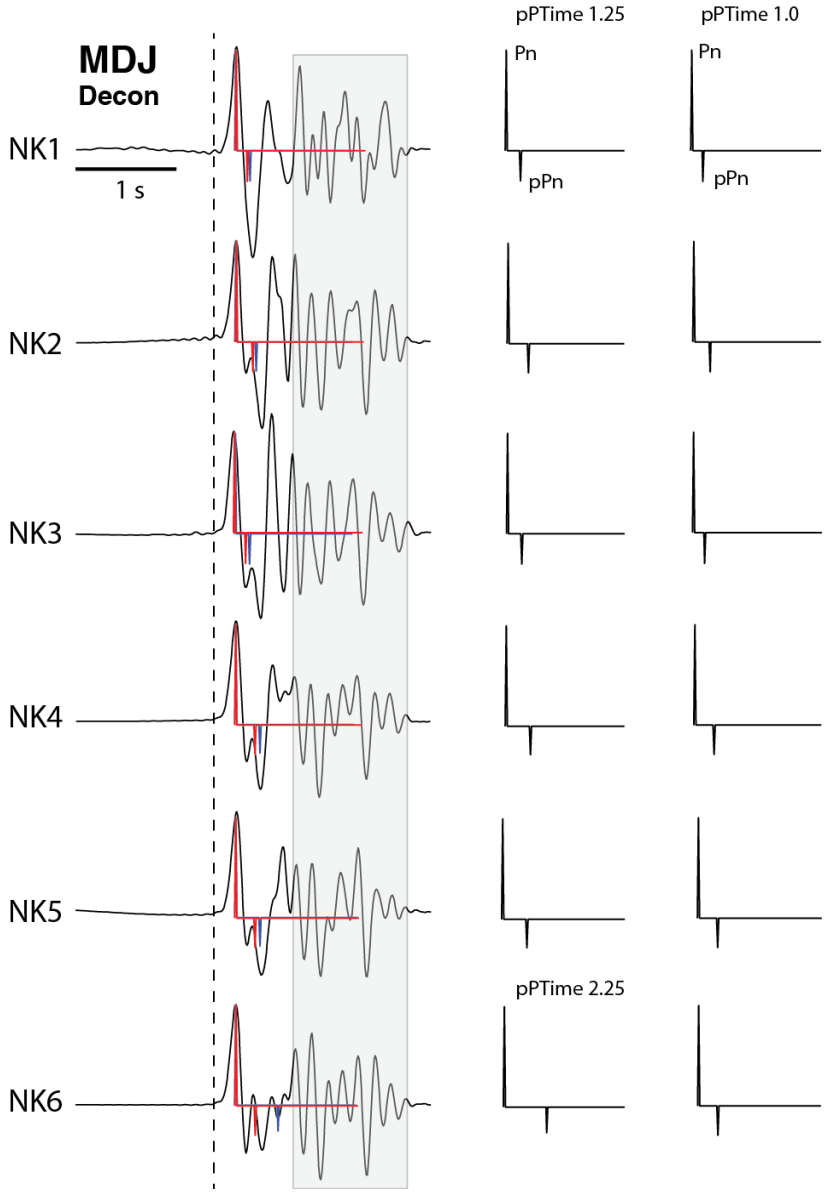

Figure 5. Comparison of the deconvolved Green's functions for MDJ with simple half-space Green's functions with elastic (pPTime 1.0) and delayed pPn (pPTime 1.25 or 2.25 times the elastic prediction). *The elastic predictions are superimposed on the data in red and the delayed pPn predictions in blue.*

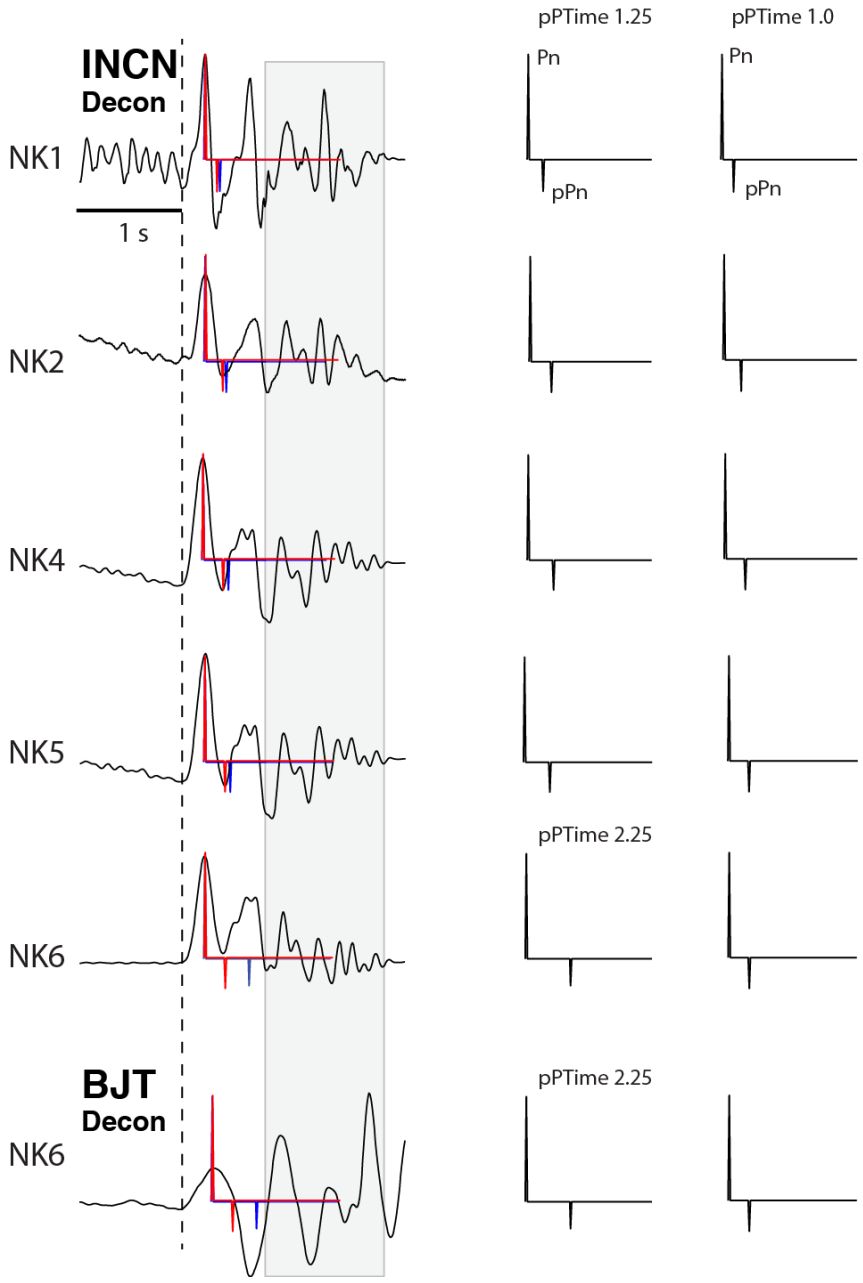

Figure 6. Comparison of the deconvolved Green's functions for INCN and BJT with simple half-space Green's functions with elastic (pPTime 1.0) and delayed pPn (pPTime 1.25 or 2.25 times the elastic prediction). *The elastic predictions are superimposed on the data in red and the delayed pPn predictions in blue.*

In contrast, the predictions for INCN for the purely elastic model and for small pPTime values are in good agreement with the timing of the weak first downswing. A half-space model appears adequate for the signals to the south from the source region, but not for signals to the north. An elastic structure that would better match the observations at MDJ was determined by forward

modeling of the estimated Green's functions, emphasizing fitting of the dovetail in the downswing of the pPn energy. The goal is to have a model that can be applied to other northerly stations. Figure 7 shows Green's function predictions for a model that appears to be adequate on average.

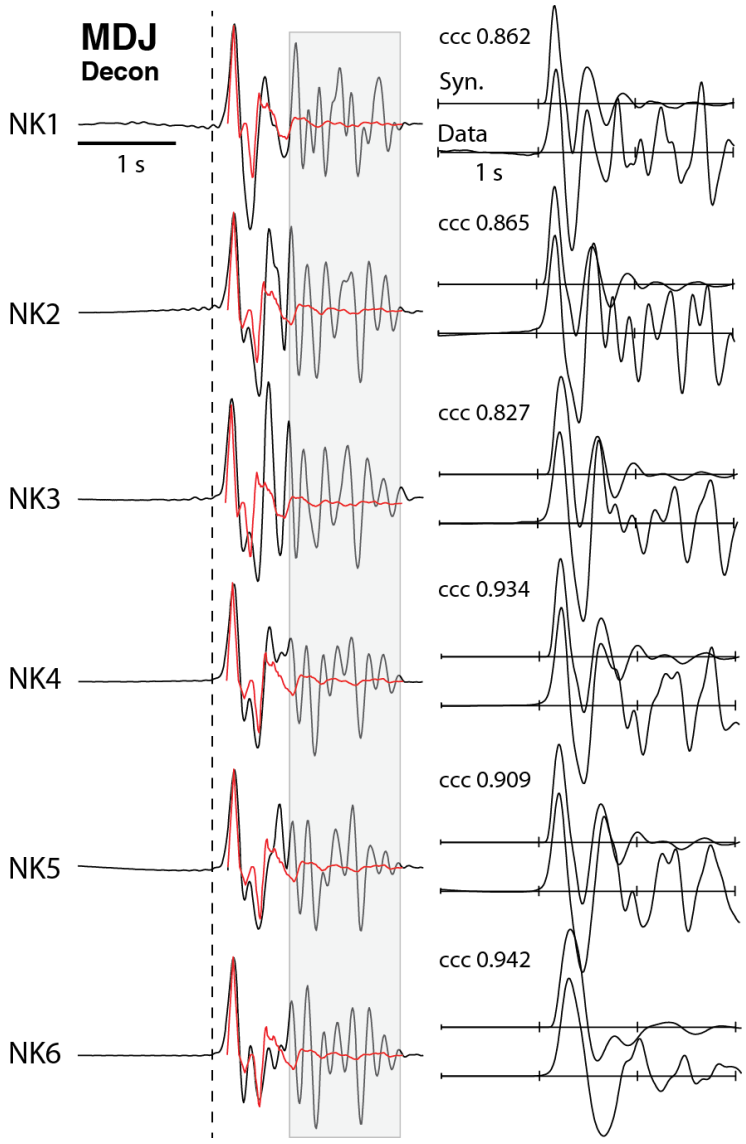

Figure 7. Comparison of deconvolved Green's functions at MDJ (black traces on the left) for the six events with prediction for a layered elastic model (Table 1), convolved with a short triangular filter (red traces). *Convolution of the model Green's functions with the RVP for each event give synthetic predictions on the right (upper traces) compared to the observed signals (lower traces), with the normalized cross correlation over the first second of the signal following the first Pn arrival being shown. The layered Green's functions are not intended to account for the signal after the first cycle and a half of the waveforms.*

The elastic model for the MDJ signals is tabulated in Table 1, and it clearly provides a much-improved fit to the dovetail feature in the waveforms for the 5 larger events than is true for the half-space models in Figure 5. The forward-modeled predictions of the observed Pn waveforms (using the source depth and source functions from the preferred models in Voytan et al. (2019)) fit the observed data quite well on average over the first cycle and a half of the signals. Later arrivals are not predicted as the path has much more complexity than can be represented by a single 1D structure.

Table 1. Velocity model from fitting of the MDJ Green's functions

Vp (km/s)	Vs (km/s)	Density (gm/cm^3)	Thickness (km)
1.50	0.866	1.20	0.01
3.20	1.848	1.60	0.25
5.50	3.175	2.55	2.8
6.00	3.460	2.60	11.0
6.70	3.870	2.80	16.0
8.00	4.620	3.30	-

This structure involves a very thin low velocity (strongly weathered) layer with a 250 m thick zone of reduced P and S velocity overlying a high velocity granitic layer. In a general sense the low velocity layers near the surface may correspond to the basalt cap layer on the north side of the mountain with strong surface weathering of the basalt. The dovetail feature arises from the underside reflections from the low velocity zone and the free surface. NK1, which is in separate mountain with no basalt layer, is not well fit by this structure, and for NK3, the source depth used appears to be about 100 m too shallow. The goal is not to attempt to uniquely characterize the near-source Green's function from the handful of signals, but to have an elastic structure compatible with the data that can be used in intercorrelations of all signals. The MDJ Pn waveforms do not indicate strongly anomalous character of the NK6 Green's function, but this likely results from the relatively large take-off angle for Pn and pPn, which cause the downgoing surface reflections to traverse intact rock largely outside of the damage zone. The same holds for the simple, half-space-like Green's functions for INCN, which do not sample the basalt layer structure to the north. Teleseismic pP will sense damage around the source volume, with steeper incidence waves (at larger teleseismic distances) being more affected.

The intercorrelation algorithm was modified to utilize multiple one-dimensional velocity structures, selecting different source structures for Voytan et al. (2019) stations at different azimuths and/or for different events at the same station. Searches were then performed to find the best explosion yields for source depths specified as in Voytan et al. (2019) based on location

in the mountain and assuming 4% tunnel grades. The intercorrelated waveforms for NK4 and NK5, found using the model in Table 1 for all stations, are shown in Figure 8.

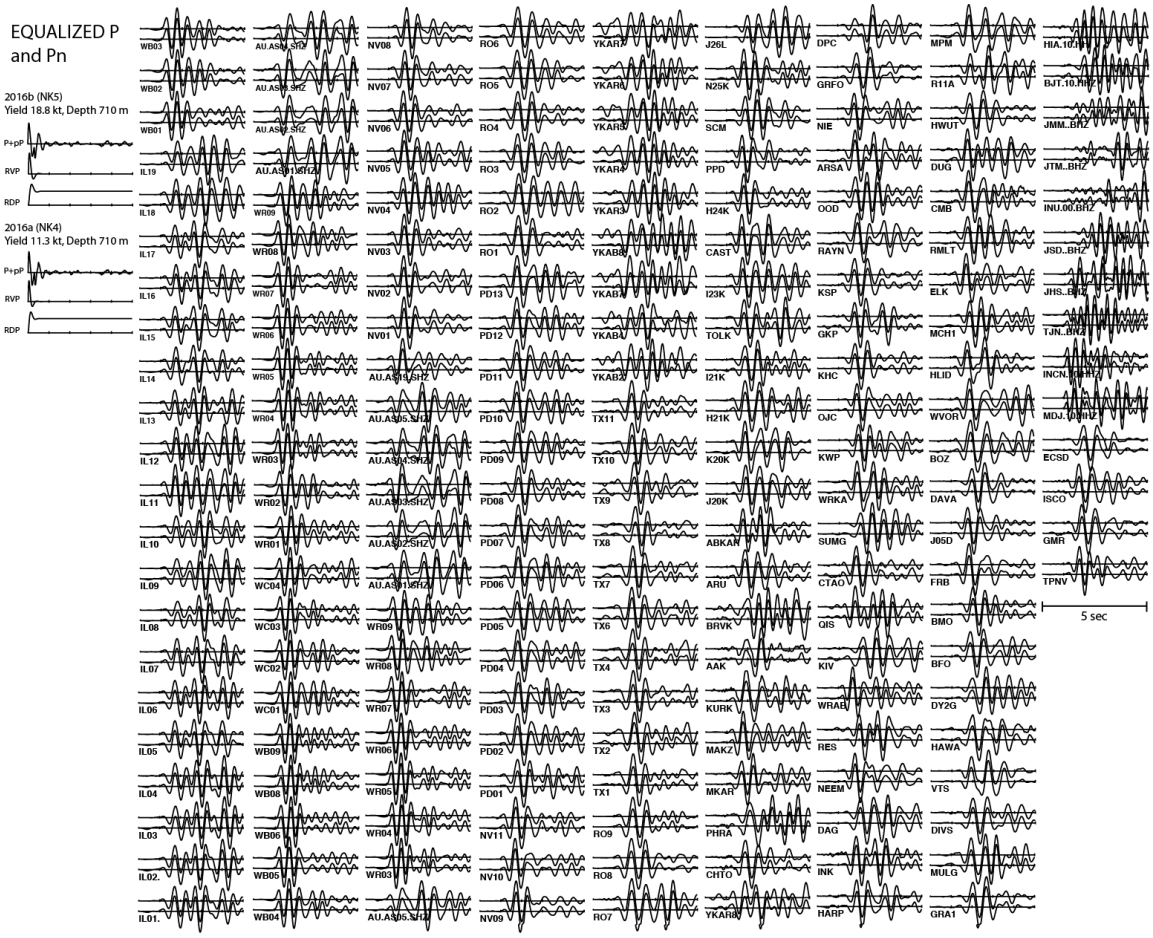

Figure 8. Equalized P and Pn waveforms for NK4 (Yield 11.3 kt, depth 710 m) and NK5 (Yield 18.8 kt, depth 710 m). *In each station pair the lower trace is the NK4 signal convolved with source function (RVP convolved with Green's function for the layered model in Table 1) for NK5, while the upper trace is the NK5 signal convolved with the source function for NK4. The yield for NK5 was held fixed and the value for NK4 determined by minimizing the amplitude weighted logarithmic average amplitude error defined by Voytan et al. (2019).*

The waveform equalization works very well for the layered crustal model, giving fits that slightly improve relative to using half-space Green's functions, with almost identical yield estimate for NK4 (11.3 kt for the layered structure versus 11.2 kt for the halfspace). Figure 8 indicates the large number of traces used to measure the relative yields. For these events, an elastic structure is viable because the damage zone is expected to be small and to have minor effects on the surface reflections.

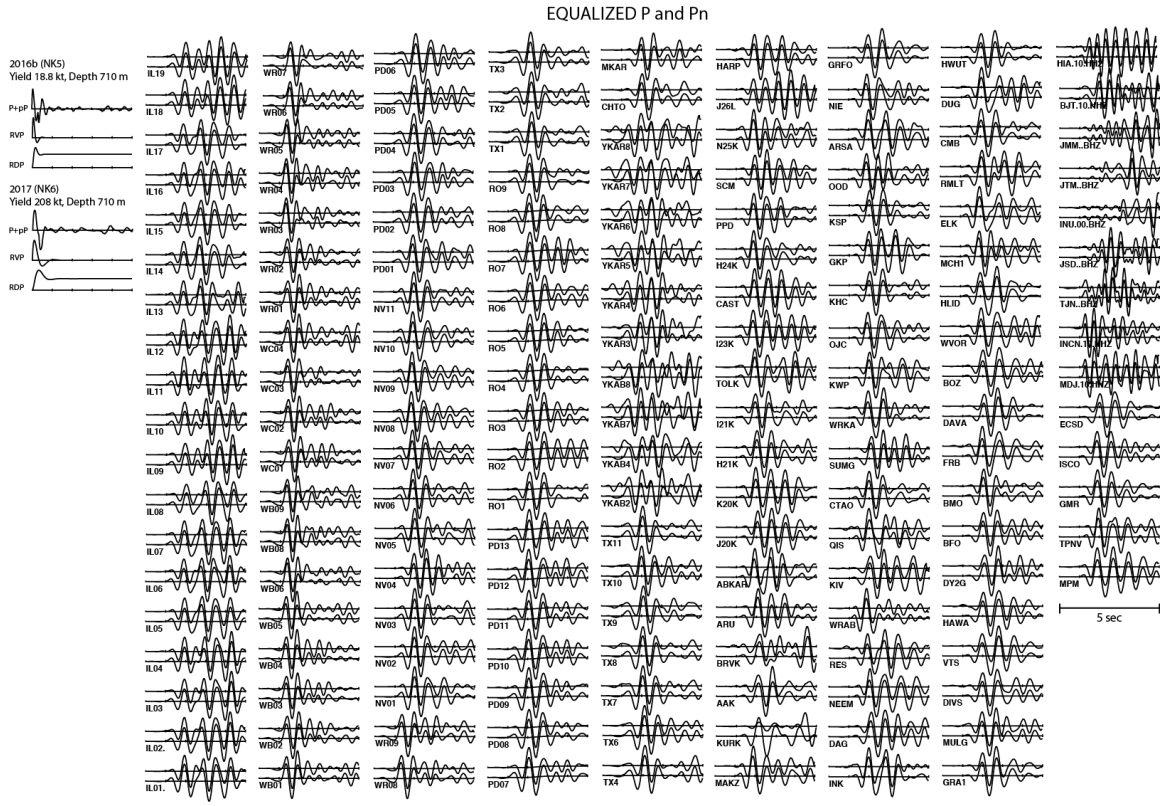

Figure 9. Equalized P and Pn waveforms for NK6 (Yield 208 kt, depth 710 m) and NK5 (Yield 18.8 kt, depth 710 m). *In each station pair the lower trace is the NK6 signal convolved with source function (RVP convolved with Green's function for the layered model in Table 1) for NK5, while the upper trace is the NK5 signal convolved with the source function for NK6. The yield for NK5 was held fixed and the value for NK6 determined by minimizing the amplitude weighted logarithmic average amplitude error defined by Voytan et al. (2019).*

Results for the NK6 event obtained relative to NK5 are shown in Figure 9. Again the equalization works very well, slightly outperforming the prior half-space results for different choices of pPTime. This stability with respect to significant differences in the Green's functions reflects a key strength of the waveform equalization approach; as long as the observations at a given station share a common Green's function, the details of the Green's function are not critical.

Intercorrelations were performed for the other three pairs of events using the structure in Table 1, with the results being tabulated in Table 2. Recognizing the azimuthal pattern between the MDJ and INCN deconvolution results, a full set of intercorrelations was run using the model in Table 1 for all azimuths from -90° to 90° (i.e., to the north), and an elastic half-space model for all stations at azimuths from 90° to 270° (i.e., to the south). These results are also tabulated in Table 2. One additional case was considered, where the same azimuthal selection of source structure

was used for NK5, but the half-space model was used for all stations for NK1. This is motivated by the distinct behavior of the MDJ and INCN deconvolutions for NK1 in Figures 3 and 4. The yield estimate for that case is also shown in Table 2. The estimates of yields are not strongly affected by the details of the source function differences, even between sources. It should be kept in mind that these results are all relative to a fixed yield estimate of 18.8 kt for NK5, and the specified source depths. Uncertainty estimates are similar to those reported by Voytan et al. (2019).

Table 2. Yield estimates for specified source depths using layered elastic Green's functions

Event	Yield, kt	Depth, m	Model Case
NK1	1.7	430	Table 1 all stations
	1.7	430	Table 1 to N, Half Space to S
	1.8	430	Half Space all stations NK1, Variable for NK5
	1.4	430	Half Space all stations (pPTime 1.25)
NK2	5.4	600	Table 1 all stations
	5.3	600	Table 1 to N, Half Space to S
	5.0	600	Half Space all stations (pPTime 1.25)
NK3	15.5	430	Table 1 all stations
	15.5	430	Table 1 to N, Half Space to S
	13.2	430	Half Space all stations (pPTime 1.25)
NK 4	11.3	710	Table 1 all stations
	11.3	710	Table 1 to N, Half Space to S
	11.2	710	Half Space all stations (pPTime 1.25)
NK 5(fixed)	18.8	710	
NK 6	208	710	Table 1 all stations
	208	710	Table 1 to N, Half Space to S
	215	710	Half Space all stations (pPTime 1.25)
	250	710	Half Space all stations (pPTime 2.25)

5. CONCLUSIONS

This final report summarizes waveform modeling and waveform equalization procedures that have provided estimates of explosion yields for the six events at the DPRK test site based on seismic wave observations combined with an explosion source model parameterization for a hard rock site. The procedure uses elastic and perturbed elastic Green's functions for half-space and plane-layered source structure for the modeling of broadband P wave signals and for the waveform equalization procedure called intercorrelation. We use a Futterman constant Q attenuation parameterization. The results have uncertainties associated with all of these choices; there are questions about the validity of the depth scaling in the Mueller-Murphy source model parameterizations, there are uncertainties in the precise geology of the source emplacements, there is clearly topography in the source region that can affect azimuthal patterns in pP surface interactions, the 2017 event appears to have created significant damage in the source environment that may not be correctly captured by the pP perturbation procedure used in the modeling, the diverse path sampling of the global data set may have skewed statistical parameters and frequency dependence of the attenuation such that use of a single t* operator leads to errors in the absolute yield estimates, etc. The analysis presented here, from the last year of the contract impacted by COVID restrictions, indicates an encouraging stability of the yield estimates from teleseismic waveform information for the six North Korean tests with respect to details of the near source crust. Deconvolution procedures for Pn phases lead to azimuthally varying elastic structures that are implemented in the teleseismic intercorrelation procedure. Yield estimates are not strongly perturbed by the use of layered source structure, largely due to the robustness of the intercorrelation procedure for events in close proximity. Futher efforts to include 3D Green's functions for rough near source topography would increase confidence in the yield estimates, but likely will not lead to significantly different results.

REFERENCES

Avants, M. S. (2005), *Effects of near-source heterogeneity on wavefields emanating from crustal sources observed at regional and teleseismic distances*, Ph.D. Thesis, Chapter 3, UCSC.

Chaves, E. J., T. Lay, and D. P. Voytan (2018), Yield estimate (230 kt) for a Mueller-Murphy model of the 3 September 2017, North Korean nuclear test (m_{bNEIC} = 6.3) from teleseismic broadband P waves assuming extensive near-source damage, *Geophys. Res. Lett.*, **45**, pp. 10,314-10,322, PDF, Supp. https://doi.org/10.1029/2018GL079343.

Lay, T. (1985), Estimating explosion yield by analytical waveform comparison, *Geophysical Journal of the Royal Astronomical Society*, **82**, pp. 1-30.

Lay, T., L. J. Burdick, and D. V. Helmberger (1984), Estimating the yields of the Amchitka tests by waveform intercorrelation, *Geophysical Journal of the Royal Astronomical Society*, **78**, pp. 181-207.

Stevens, J. L. and M. O'Brien (2018), 3D nonlinear calculation of the 2017 North Korean nuclear test, *Seismological Research Letters*, **89**, pp. 2068-2077, https://doi.org/10.1785/0220180099.

Voytan, D. P., T. Lay, E. J. Chaves, and J. T. Ohman (2019), Yield estimates for the six North Korean nuclear tests from teleseismic P wave modeling and intercorrelation of P and Pn recordings, *Journal of Geophysical Research: Solid Earth*, **124**, pp. 4916-4939, PDF, Supp. https://doi.org/10.1029/2019JB017418.

LIST OF SYMBOLS, ABBREVIATIONS, AND ACRONYMS

BJT Seismic Station Baijiatuan, Beijing, China

DPRK Democratic People's Republic of Korea

INCN Seismic Station Inchon, Republic of Korea

JVE Joint Verification Experiment

LLNL Lawrence Livermore National Laboratory

MDJ Seismic Station Mudanjiang, Heilongjiang Province, China

RVP Reduced Velocity Potential

Approved for public release; distribution is unlimited.

DISTRIBUTION LIST

DTIC/OCP
8725 John J. Kingman Rd, Suite 0944 Ft
Belvoir, VA 22060-6218 1 cy

AFRL/RVIL
Kirtland AFB, NM 87117-5776 1 cy

Official Record Copy
AFRL/RVB/Dr. Raymond J. Willemann 1 cy